



HAL
open science

On the Degrees of Freedom of RIS-Aided Holographic MIMO Systems

Juan Carlos Ruiz-Sicilia, xuewen qian, Marco Di Renzo, Vincenzo Sciancalepore, Merouane Debbah, Xavier Costa-Perez

► **To cite this version:**

Juan Carlos Ruiz-Sicilia, xuewen qian, Marco Di Renzo, Vincenzo Sciancalepore, Merouane Debbah, et al.. On the Degrees of Freedom of RIS-Aided Holographic MIMO Systems. 26th International ITG Workshop on Smart Antennas and 13th Conference on Systems, Communications, and Coding, Feb 2023, Brunswick, Germany. hal-04186798

HAL Id: hal-04186798

<https://centralesupelec.hal.science/hal-04186798>

Submitted on 24 Aug 2023

HAL is a multi-disciplinary open access archive for the deposit and dissemination of scientific research documents, whether they are published or not. The documents may come from teaching and research institutions in France or abroad, or from public or private research centers.

L'archive ouverte pluridisciplinaire **HAL**, est destinée au dépôt et à la diffusion de documents scientifiques de niveau recherche, publiés ou non, émanant des établissements d'enseignement et de recherche français ou étrangers, des laboratoires publics ou privés.

On the Degrees of Freedom of RIS-Aided Holographic MIMO Systems

Juan Carlos Ruiz-Sicilia, Xuewen Qian, Marco Di Renzo, Vincenzo Sciancalepore,
Merouane Debbah, and Xavier Costa-Perez

Abstract—In this paper, we study surface-based communication systems based on different levels of channel state information for system optimization. We analyze the system performance in terms of rate and degrees of freedom (DoF). We show that the deployment of a reconfigurable intelligent surface (RIS) results in increasing the number of DoF, by extending the near-field region. Over Rician fading channels, we show that an RIS can be efficiently optimized only based on the positions of the transmitting and receiving surfaces, while providing good performance if the Rician fading factor is not too small.

Index Terms—Reconfigurable intelligent surfaces, holographic multiple-antenna systems, degrees of freedom.

I. INTRODUCTION

The fifth generation (5G) of wireless networks is being deployed providing improved system performance. However, the development of emerging applications, such as the Industrial Internet of Things (IIoT), requires ever more demanding performance in terms of rate, reliability, and number of users/devices to serve [1]. Experimental trials and system-level simulations have shown that the performance of current wireless systems, based on optimizing only the transmitters and receivers, can be further improved by considering the environment as an additional optimization variable [2]–[4]. Motivated by these considerations, a new paradigm named intelligent reconfigurable environment (IRE) [5]–[7] has emerged as a new approach to overcome current design principles. In an IRE, the propagation of the electromagnetic waves can be optimized in order to make the wireless channel between transmitters and receivers more reliable, while reducing the implementation complexity of transmitters and receivers. The control of the environment is carried out by using transmitting, receiving, and reflecting surfaces based on programmable metamaterials. These surfaces can be either active or nearly-passive. Active surfaces that operate as transmitters and receivers are referred

to as holographic surfaces (HoloS) [8]. Nearly-passive surfaces that operate as, e.g., reflecting or refracting surfaces, are referred to as reconfigurable intelligent surfaces (RIS) [9], [10].

HoloS can be utilized as flexible antennas that are electrically large. Their large size compared to the wavelength increases the Fraunhofer distance, making the plane wave far-field assumption no longer valid in many scenarios, especially for operation at very high frequency bands [11]. In this case, the wavefront of the electromagnetic waves is not planar anymore, which opens new communication opportunities, e.g., the possibility of spatial multiplexing even in line-of-sight (LoS) multiple-input multiple-output (MIMO) channels [12], [13]. RIS can be utilized, on the other hand, to establish strong transmission links by appropriately shaping the signals reflected or refracted by existing material objects, in order to, e.g., solve coverage hole problems [9], [10]. The combination of HoloS and RIS enables the transmission through high-rank channels ensuring high signal-to-noise ratio (SNR) links, eventually leading to high capacity gains.

In this paper, motivated by these considerations, we analyze different strategies to optimize an RIS-aided HoloS communication system as a function of the level of channel state information (CSI) for optimizing the RIS. In particular, we focus our attention on the achievable number of degrees of freedom (DoF) under different scenarios [11]. To this end, the paper is organized as follows. Section II introduces the surface-based communication system model. Section III summarizes the considered RIS configurations as a function of the available CSI. Section IV presents some numerical results to compare the rate and the DoF of the considered case studies. Finally, Section V concludes the paper.

Notation: Bold lower and upper case letters represent vectors and matrices, respectively. $\mathbb{C}^{a \times b}$ denotes the space of complex matrices of dimensions $a \times b$. $(\cdot)^*$ and $(\cdot)^H$ represent the complex conjugate and the Hermitian transpose. $\text{diag}(\mathbf{x})$ denotes the square diagonal matrix which has the elements of \mathbf{x} on the main diagonal. $\text{Tr}(\mathbf{X})$ is the trace of matrix \mathbf{X} , and $\mathbb{E}\{\cdot\}$ stands for the expectation operator. The notation $\mathbf{A} \succeq (\succ) \mathbf{B}$ means that $\mathbf{A} - \mathbf{B}$ is positive semidefinite (definite). $\nabla_{\mathbf{x}} f(\cdot)$ is the gradient of f with respect to $\mathbf{X}^* \in \mathbb{C}^{a \times b}$, which also lies in $\mathbb{C}^{a \times b}$. $\mathbf{A}(i, k)$ denotes the k -th element of the i -th row of matrix \mathbf{A} . j is the imaginary unit. $\mathcal{CN}(\bar{x}, \sigma^2)$ denotes the complex Gaussian distribution with mean \bar{x} and variance σ^2 .

J. C. Ruiz-Sicilia and M. Di Renzo are with Université Paris-Saclay, CNRS, CentraleSupélec, Laboratoire des Signaux et Systèmes, 91192 Gif-sur-Yvette, France. (juan-carlos.ruiz-sicilia@centralesupelec.fr). X. Qian was with Université Paris-Saclay, CNRS, CentraleSupélec, Laboratoire des Signaux et Systèmes, 91192 Gif-sur-Yvette, France, when this work was done. V. Sciancalepore is with NEC Laboratories Europe GmbH, Germany. M. Debbah is with the Technology Innovation Institute, Abu Dhabi, United Arab Emirates. X. Costa-Pérez is with the i2cat Research Center, Spain, with the Catalan Institution for Research and Advanced Studies (ICREA), Spain, and with NEC Laboratories Europe GmbH, Germany. This work was supported in part by the European Commission through the H2020 MSCA 5GSmartFact project under grant agreement number 956670, the NEC Student Research Fellowship program, the H2020 ARIADNE project under grant agreement number 871464, and the H2020 RISE-6G project under grant agreement number 101017011.

II. SYSTEM MODEL

We consider an RIS-aided HoloS communication system as illustrated in Fig. 1. The transmitter and receiver are modeled as uniform rectangular arrays (URAs) with $L = L_y L_z$ and $M = M_y M_z$ antenna elements, respectively, where L_y (M_y) and L_z (M_z) are the numbers of antenna elements on the y -axis and z -axis. G_t and G_r denote the gains of the antenna elements at the transmitter and receiver, respectively. The transmitter and receiver are placed on vertical walls parallel to each other. D denotes the distance between these walls.

The RIS consists of N_x unit cells on the x -axis and N_y unit cells on the y -axis (i.e., $N = N_x N_y$ is the total number of unit cells). The RIS is installed on a vertical wall that is perpendicular to the HoloS transmitter and HoloS receiver, and the distance between the center of the RIS and the plane containing the HoloS is d_{ris} . The distance between the center of the transmitting HoloS and the plane containing the RIS is l_t , and the distance between the midpoint of the receiving HoloS and the plane containing the RIS is l_r .

For simplicity, we assume that the three surfaces are at the same height. In the three surfaces, the centers between adjacent elements are separated by $d = \lambda/2$ to avoid the mutual coupling among them, where λ is the wavelength. Thus, the area of each element is $S_c = \lambda^2/4$. The position of the l -th transmitting element, the m -th receiving element, and the n -th unit cell of the RIS are denoted by $\mathbf{r}_t^l = (x_t^l, y_t^l, z_t^l)$, $\mathbf{r}_r^m = (x_r^m, y_r^m, z_r^m)$ and $\mathbf{r}_{\text{ris}}^n = (x_{\text{ris}}^n, y_{\text{ris}}^n, z_{\text{ris}}^n)$, respectively. The positions can be formulated as follows:

$$\mathbf{r}_t^l = \left(-d_{\text{ris}}, dl_y - \frac{d}{2}(L_y + 1), l_t + dl_z - \frac{d}{2}(L_z + 1) \right) \quad (1)$$

$$\mathbf{r}_r^m = \left(D - d_{\text{ris}}, dm_y - \frac{d}{2}(M_y + 1), l_r + dm_z - \frac{d}{2}(M_z + 1) \right) \quad (2)$$

$$\mathbf{r}_{\text{ris}}^n = \left(n_x d - \frac{d}{2}(N_x + 1), n_y d - \frac{d}{2}(N_y + 1), 0 \right) \quad (3)$$

where $l = (l_z - 1)L_z + l_y$, $m = (m_z - 1)M_z + m_y$ and $n = (n_x - 1)N_x + n_y$, and l_z (m_z) and l_y (m_y) denote the indices of the URAs along the z -axis and y -axis, respectively. Similarly, n_x and n_y denote the indices of the unit cells of the RIS along the x -axis and y -axis.

As for the RIS, we consider the canonical reflectarray-based model [14], according to which the reflection coefficients of the N unit cells are denoted by the vector $\boldsymbol{\theta} = \text{diag}([e^{j\theta_1}, e^{j\theta_2}, \dots, e^{j\theta_N}])$, where $\theta_n \in [-\pi, \pi]$ is the phase shift applied by the n -th unit cell. The direct channel between the transmitting and receiving HoloS is denoted by $\mathbf{H}_{\text{dir}} \in \mathbb{C}^{M \times L}$. The channel from the transmitting HoloS to the RIS and the channel from the RIS to the receiving HoloS are denoted by $\mathbf{H} \in \mathbb{C}^{N \times L}$ and $\mathbf{G} \in \mathbb{C}^{M \times N}$, respectively. Then, the signal \mathbf{y} at the receiver is given by:

$$\mathbf{y} = (\mathbf{H}_{\text{dir}} + \mathbf{G}\boldsymbol{\theta}\mathbf{H})\mathbf{x} + \boldsymbol{\omega} \quad (4)$$

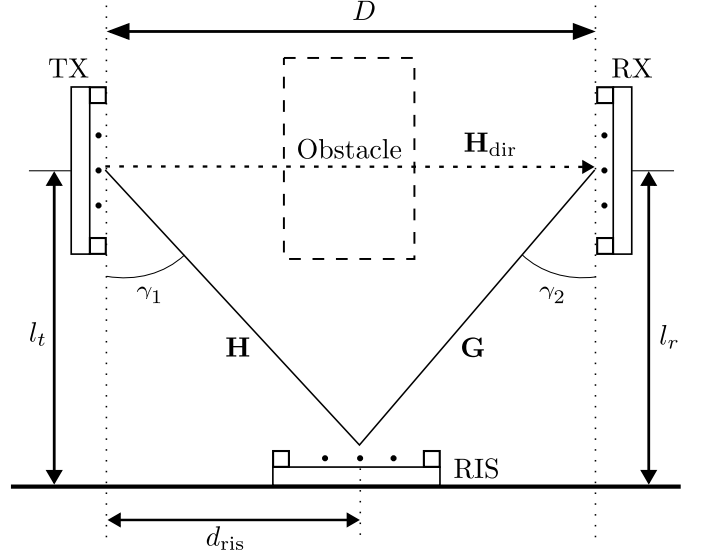


Fig. 1: Top view of the considered communication system model [15].

where $\boldsymbol{\omega}$ denotes the white additive Gaussian noise with zero means and variance σ^2 , i.e., $\mathbb{E}\{\boldsymbol{\omega}\boldsymbol{\omega}^H\} = \sigma^2\mathbf{I}_M$ and \mathbf{x} denotes the transmitted signal. The symbols in \mathbf{x} are distributed according to a circularly symmetric complex Gaussian distribution with $\mathbb{E}\{\mathbf{x}\mathbf{x}^H\} = \mathbf{Q}$, where \mathbf{Q} is the covariance matrix. Assuming that the maximum transmit power is P_T , we obtain $\text{Tr}(\mathbf{Q}) \leq P_T$.

Given this system model, the achievable rate can be written as:

$$R(\boldsymbol{\theta}, \mathbf{Q}) = \log_2 \left| \mathbf{I} + \frac{(\mathbf{H}_{\text{dir}} + \mathbf{G}\boldsymbol{\theta}\mathbf{H})\mathbf{Q}(\mathbf{H}_{\text{dir}} + \mathbf{G}\boldsymbol{\theta}\mathbf{H})^H}{\sigma^2} \right| \quad (5)$$

A. Channel Model

The links between each pair of surfaces are modeled as Rician channels with Rician factor K . Hence, the channels can be formulated as follows:

$$\mathbf{G} = \sqrt{\frac{K}{K+1}}\mathbf{G}^{\text{LoS}} + \sqrt{\frac{1}{K+1}}\mathbf{G}^{\text{NLoS}} \quad (6)$$

$$\mathbf{H} = \sqrt{\frac{K}{K+1}}\mathbf{H}^{\text{LoS}} + \sqrt{\frac{1}{K+1}}\mathbf{H}^{\text{NLoS}} \quad (7)$$

where \mathbf{G}^{LoS} (\mathbf{H}^{LoS}) and \mathbf{G}^{NLoS} (\mathbf{H}^{NLoS}) denote the LoS and the non-line-of-sight (NLoS) components of each channel, respectively.

The LoS component of the channel from the l -th element of the transmitting HoloS to the n -th unit cell of the RIS can be formulated as [16, Eq. (5)]:

$$\mathbf{H}^{\text{LoS}}(n, l) = \sqrt{\frac{G_t S_c \cos \gamma_1}{4\pi (d_1(n, l))^2}} e^{jk_0 d_1(n, l)} \quad (8)$$

where $G_c = S_c 4\pi/\lambda^2$, $k_0 = 2\pi/\lambda$, $\cos \gamma_1 = z_t^l/d_1(n, l)$ and

$$d_1(n, l) = \sqrt{(x_t^l - x_{\text{ris}}^n)^2 + (y_t^l - y_{\text{ris}}^n)^2 + (z_t^l - z_{\text{ris}}^n)^2} \quad (9)$$

Similarly, the LoS component of the channel from the n -th unit cell of the RIS to the m -th element of the receiving HoloS can be expressed as follows [16, Eq. (6)]:

$$\mathbf{G}^{\text{LoS}}(m, n) = \sqrt{\frac{G_r S_c \cos \gamma_2}{4\pi (d_2(m, n))^2}} e^{jk_0 d_2(m, n)} \quad (10)$$

where $\cos \gamma_2 = z_r^m / d_2(m, n)$ and

$$d_2(m, n) = \sqrt{(x_l^r - x_{\text{ris}}^n)^2 + (y_l^r - y_{\text{ris}}^n)^2 + (z_l^r - z_{\text{ris}}^n)^2} \quad (11)$$

The NLoS components of the channels can be formulated as follows:

$$\mathbf{G}^{\text{NLoS}}(m, n) = |\mathbf{G}^{\text{LoS}}(m, n)| x_{m, n} \quad (12)$$

$$\mathbf{H}^{\text{NLoS}}(n, l) = |\mathbf{H}^{\text{LoS}}(n, l)| x_{n, l} \quad (13)$$

where $x_{m, n}$ and $x_{n, l}$ are independent and identically distributed standard Gaussian random variables, i.e., $x_{m, n}, x_{n, l} \sim \mathcal{CN}(0, 1)$.

As far as the direct channel is concerned, we have:

$$\mathbf{H}_{\text{dir}} = \sqrt{\frac{K}{K+1}} \mathbf{H}_{\text{dir}}^{\text{LoS}} + \sqrt{\frac{1}{K+1}} \mathbf{H}_{\text{dir}}^{\text{NLoS}} \quad (14)$$

where $\mathbf{H}_{\text{dir}}^{\text{LoS}}$ and $\mathbf{H}_{\text{dir}}^{\text{NLoS}}$ denote the LoS and NLoS components, respectively.

The LoS component can be written as follows:

$$\mathbf{H}_{\text{dir}}(m, l) = \sqrt{\frac{G_t G_r \lambda^2}{(4\pi)^2 (d_{\text{dir}}(n, m))^{\alpha_{\text{dir}}}}} e^{jk_0 d_{\text{dir}}(n, m)} \quad (15)$$

where α_{dir} is the path loss exponent and

$$d_{\text{dir}}(n, m) = \sqrt{(x_t^l - x_r^m)^2 + (y_t^l - y_r^m)^2 + (z_t^l - z_r^m)^2} \quad (16)$$

Similarly, the NLoS component $\mathbf{H}_{\text{dir}}^{\text{NLoS}}$ can be formulated as:

$$\mathbf{H}_{\text{dir}}^{\text{NLoS}}(m, l) = |\mathbf{H}_{\text{dir}}^{\text{LoS}}(m, l)| x_{m, l} \quad (17)$$

where $x_{m, l} \sim \mathcal{CN}(0, 1)$.

III. PROBLEM FORMULATION

In this section, we consider several case studies for optimizing the transmitting and receiving HoloS, and the RIS as a function of the CSI that is needed for optimizing the RIS. On the other hand, we assume that the transmitting and receiving HoloS have perfect CSI. It is known, in fact, that the bottleneck when optimizing RIS-aided systems is given by the overhead for configuring the RIS because of its nearly-passive implementation [17].

To make the problem formulation parametric as a function of the CSI assumed for optimizing the RIS, the objective function in (5) is rewritten as a function of three generic channel matrices \mathbf{F}_1 , \mathbf{F}_2 and \mathbf{F}_3 , as follows:

$$f(\boldsymbol{\theta}, \mathbf{Q}; \mathbf{F}_1, \mathbf{F}_2, \mathbf{F}_3) = \log_2 \left| \mathbf{I} + \frac{(\mathbf{F}_1 + \mathbf{F}_3 \boldsymbol{\theta} \mathbf{F}_2) \mathbf{Q} (\mathbf{F}_1 + \mathbf{F}_3 \boldsymbol{\theta} \mathbf{F}_2)^H}{\sigma^2} \right| \quad (18)$$

The three matrices \mathbf{F}_1 , \mathbf{F}_2 and \mathbf{F}_3 are specialized for each considered case study in the following subsections. With the notation in (18), we mean that the phase shifts of the RIS are optimized assuming that \mathbf{F}_1 , \mathbf{F}_2 and \mathbf{F}_3 are known.

Based on (18), the optimization problem of interest can be stated as follows:

$$\underset{\boldsymbol{\theta}, \mathbf{Q}}{\text{maximize}} f(\boldsymbol{\theta}, \mathbf{Q}; \mathbf{F}_1, \mathbf{F}_2, \mathbf{F}_3) \quad (19a)$$

$$\text{subject to } \text{Tr}(\mathbf{Q}) \leq P_t; \mathbf{Q} \succeq \mathbf{0}; \quad (19b)$$

$$|\boldsymbol{\theta}(n, n)| = 1, n = 1, 2, \dots, N \quad (19c)$$

In [15], the authors introduce an algorithm to solve the problem in (19) based on the projected gradient method (PGM). The approach proposed in [15] employs one step size to optimize \mathbf{Q} and $\boldsymbol{\theta}$ in an iterative manner. The proposed algorithm needs a careful choice of the step size. To this end, the authors introduce a scaling factor that needs to be finely tuned depending on the considered scenario. A more efficient solution is proposed in [18], where the authors generalize the approach in [15] by using two different step sizes for optimizing $\boldsymbol{\theta}$ and \mathbf{Q} . This approach avoids the need of finely tuning an ad hoc scaling factor for each considered scenario.

Inspired by [18], we propose the following iterative algorithm to solve the problem in (19):

$$\boldsymbol{\theta}_{n+1} = P_{\Theta}(\boldsymbol{\theta}_n + \mu_1 \nabla_{\boldsymbol{\theta}} f(\boldsymbol{\theta}_n, \mathbf{Q}_n; \mathbf{F}_1, \mathbf{F}_2, \mathbf{F}_3)) \quad (20a)$$

$$\mathbf{Q}_{n+1} = P_{\mathbf{Q}}(\mathbf{Q}_n + \mu_2 \nabla_{\mathbf{Q}} f(\boldsymbol{\theta}_{n+1}, \mathbf{Q}_n; \mathbf{F}_1, \mathbf{F}_2, \mathbf{F}_3)) \quad (20b)$$

where $P_{\Theta}(\cdot)$ and $P_{\mathbf{Q}}(\cdot)$ denote the projection onto the feasible sets of $\boldsymbol{\theta}$ and \mathbf{Q} , respectively. The gradients and the projections can be found in [15, Eqs. (17a), (17b), (18), (21)].

In (20), μ_1 and μ_2 denote the step sizes, which need to be carefully chosen in order to ensure convergence. For this purpose, we implement the Armijo-Goldstein backtracking line search to adjust the largest possible step size in each iteration of the algorithm [18]. To this end, we define $L_1, L_2 > 0$ as the maximum initial step sizes and $\rho_1, \rho_2 \in (0, 1)$ as the search control parameters. The backtracking line search method consists of replacing μ_1 and μ_2 with $L_1 \rho_1^{\alpha_n}$ and $L_2 \rho_2^{\beta_n}$, respectively, where α_n and β_n are the minimum non-negative integer values fulfilling the conditions:

$$f(\boldsymbol{\theta}_{n+1}, \mathbf{Q}_n; \mathbf{F}_1, \mathbf{F}_2, \mathbf{F}_3) \leq f(\boldsymbol{\theta}_n, \mathbf{Q}_n; \mathbf{F}_1, \mathbf{F}_2, \mathbf{F}_3) - \delta_1 \|\boldsymbol{\theta}_{n+1} - \boldsymbol{\theta}_n\|^2 \quad (21)$$

$$f(\boldsymbol{\theta}_{n+1}, \mathbf{Q}_{n+1}; \mathbf{F}_1, \mathbf{F}_2, \mathbf{F}_3) \leq f(\boldsymbol{\theta}_{n+1}, \mathbf{Q}_n; \mathbf{F}_1, \mathbf{F}_2, \mathbf{F}_3) - \delta_2 \|\mathbf{Q}_{n+1} - \mathbf{Q}_n\|^2 \quad (22)$$

with being $\delta_1, \delta_2 > 0$ small constants.

A. Scheme 1: Optimization Based on Perfect CSI

This is the benchmark scheme (optimal configuration), where it is assumed that perfect CSI is available for optimizing the RIS, i.e., \mathbf{H}_{dir} , \mathbf{H} and \mathbf{G} are assumed to be known. The optimal values of $\boldsymbol{\theta}^{\text{opt}}$ and \mathbf{Q}^{opt} are obtained solving (19) with the proposed algorithm and by setting $\mathbf{F}_1 = \mathbf{H}_{\text{dir}}$, $\mathbf{F}_2 = \mathbf{H}$, $\mathbf{F}_3 = \mathbf{G}$.

B. Scheme 2: Optimization Based on LoS CSI

In this case, we assume that the RIS is optimized only based on the prior knowledge of the LoS components of the channels, i.e., $\mathbf{H}_{\text{dir}}^{\text{LoS}}$, \mathbf{H}^{LoS} and \mathbf{G}^{LoS} . Specifically, the optimization is carried out in two steps.

Firstly, the RIS vector of the phase shifts of the RIS is optimized by solving (19) with the proposed algorithm and setting $\mathbf{F}_1 = \mathbf{H}_{\text{dir}}^{\text{LoS}}$, $\mathbf{F}_2 = \mathbf{H}^{\text{LoS}}$, $\mathbf{F}_3 = \mathbf{G}^{\text{LoS}}$. The obtained solution is denoted as $\boldsymbol{\theta}^{\text{LoS}}$. It is worth mentioning that in this step the covariance matrix \mathbf{Q} is optimized as well. However, the obtained matrix is disregarded.

Secondly, once the RIS is optimized, the end-to-end channel is $\tilde{\mathbf{H}} = \mathbf{H}_{\text{dir}} + \mathbf{G}\boldsymbol{\theta}^{\text{LoS}}\mathbf{H}$. Based on this channel, the covariance matrix \mathbf{Q} can be obtained by applying the water-filling solution [12], under the assumption that all the channels are perfectly known at the transmitting and receiving HoloS. By applying the singular value decomposition (SVD) to the end-to-end channel $\tilde{\mathbf{H}}$, we obtain $\tilde{\mathbf{H}} = \mathbf{U}\mathbf{S}\mathbf{V}^H$ with $\mathbf{S} = \text{diag}(\lambda_1, \lambda_2, \dots, \lambda_{N_s})$, $\mathbf{V} \in \mathbb{C}^{L \times N_s}$, and $N_s \leq \min(M, L)$. Then, the optimal \mathbf{Q}^{LoS} is given by:

$$\mathbf{Q}^{\text{LoS}} = \mathbf{V} \text{diag}(P_{T,1}, P_{T,2}, \dots, P_{T,N_s}) \mathbf{V}^H \quad (23)$$

where $P_{T,k}$ is the power allocated to the k -th communication mode, which is given by $P_{T,k} = \max(\mu - \frac{\sigma^2}{\lambda_k^2}, 0)$ with μ chosen to fulfill the condition $\sum_{k=1}^{k=N_s} P_{T,k} = P_T$.

C. Scheme 3: Optimization Based on Location Information

This case study is motivated by the focusing function introduced in [19] and, later, studied in [20] and [21] for RIS-aided LoS channels. Similar to Scheme 3, we assume that the RIS is optimized only based on the LoS components of the channel. However, we further relax the prior knowledge for optimizing the RIS and assume that $\boldsymbol{\theta}$ is optimized only based on the knowledge for the center positions of the transmitting and receiving HoloS.

Specifically, inspired by the concept of focusing function defined in [19], the channel phase of the direct channel between the center points of the transmitting and receiving HoloS can be written as follows:

$$\Phi_{\text{dir}} = k_0 d_{\text{dir}} = k_0 \sqrt{D^2 + (l_t - l_r)^2} \quad (24)$$

Likewise, the accumulated channel phase of the link between the center point of the transmitting HoloS and the n -th unit cell of the RIS and from the n -th unit cell of the RIS to the center point of the receiving HoloS can be expressed as:

$$\Phi_{\text{indir}}^{\text{focus}}(n) = k_0 d_1^{\text{focus}}(n) + \boldsymbol{\theta}(n, n) + k_0 d_2^{\text{focus}}(n) \quad (25)$$

where

$$d_1^{\text{focus}}(n) = \sqrt{(-d_{\text{ris}} - x_n^{\text{ris}})^2 + (y_n^{\text{ris}})^2 + l_t^2} \quad (26)$$

$$d_2^{\text{focus}}(n) = \sqrt{(D - d_{\text{ris}} - x_n^{\text{ris}})^2 + (y_n^{\text{ris}})^2 + l_r^2} \quad (27)$$

In this case study, we assume that the phase shifts of the RIS are optimized to compensate for the phase shifts $\Phi_{\text{indir}}^{\text{focus}}(n)$, so that all the reflected signals reach the receiving HoloS with the

same phase as the direct channel, i.e., $\Phi_{\text{dir}} = \Phi_{\text{indir}}^{\text{focus}}(n)$ for $n \in [1, N]$. Hence, the n -th element of the phase shift vector of the RIS can be formulated as follows:

$$\boldsymbol{\theta}^{\text{focus}}(n, n) = k_0(d_{\text{dir}} - d_1^{\text{focus}}(n) - d_2^{\text{focus}}(n)) \quad (28)$$

Once the RIS is optimized, the end-to-end channel is given and known. Thus, \mathbf{Q} is optimized as for Scheme 2.

D. Scheme 4: Far-Field Optimization (Anomalous Reflection)

In this case study, we optimize $\boldsymbol{\theta}$ and \mathbf{Q} as for Scheme 3 under the assumption that the transmitting and receiving HoloS are in the far-field of each other and of the RIS.

Therefore, the distances in (26) and (27) can be simplified. Let us consider (26). We can rewrite it as follows:

$$\begin{aligned} d_1^{\text{focus}}(n) &= \sqrt{d_{\text{ris}}^2 + 2d_{\text{ris}}x_{\text{ris}}^n + (x_{\text{ris}}^n)^2 + (y_{\text{ris}}^n)^2 + l_t^2} \\ &= d_1 \sqrt{1 + \frac{2d_{\text{ris}}x_{\text{ris}}^n + (x_{\text{ris}}^n)^2 + (y_{\text{ris}}^n)^2}{d_1^2}} \end{aligned} \quad (29)$$

where $d_1 = \sqrt{d_{\text{ris}}^2 + l_t^2}$.

Under the assumption of far-field propagation, we have:

$$d_1 \gg x_{\text{ris}}^n, y_{\text{ris}}^n \quad (30)$$

which results in:

$$d_1^{\text{far}}(n) \approx d_1 + \frac{d_{\text{ris}}x_{\text{ris}}^n}{d_1} \quad (31)$$

By applying the same approximation to (27), we obtain:

$$d_2^{\text{far}}(n) \approx d_2 - \frac{(D - d_{\text{ris}})x_{\text{ris}}^n}{d_2} \quad (32)$$

where $d_2 = \sqrt{(D - d_{\text{ris}})^2 + l_r^2}$.

By using the same line of thought as for Scheme 3, we have:

$$\boldsymbol{\theta}^{\text{far}}(n, n) = k_0(d_{\text{dir}} - d_1^{\text{far}}(n) - d_2^{\text{far}}(n)). \quad (33)$$

Once the RIS is optimized, the end-to-end channel is given and known. Thus, \mathbf{Q} is optimized as for Scheme 2 and Scheme 3.

IV. NUMERICAL RESULTS

In this section, we illustrate some numerical results to analyze the performance of the considered case studies. We assume a setup in which the transmitting and receiving HoloS are equipped with 8×8 elements. The simulation parameters are as follows: $l_t = 2$ m, $l_r = 2$ m, $G_t = 3$ dBi, $G_r = 3$ dBi, $f = 3.5$ GHz, $P_T = -10$ dBm, and $\alpha_{\text{dir}} = 3$. We consider a noise spectral density $N_0 = -170$ dBm/Hz and a transmission bandwidth $BW = 20$ MHz resulting in a noise variance $\sigma^2 = N_0 BW = -97$ dBm.

In Fig. 2, we show the achievable rate as a function of the number of unit cells of the RIS, by assuming that the direct channel is blocked by an obstacle, and $d_{\text{ris}} = D/2$ with $D = 15$ m. As expected, the rate increases for smaller values of K , since the channel is richer in terms of multipaths and the number of DoF increases. However, it is important

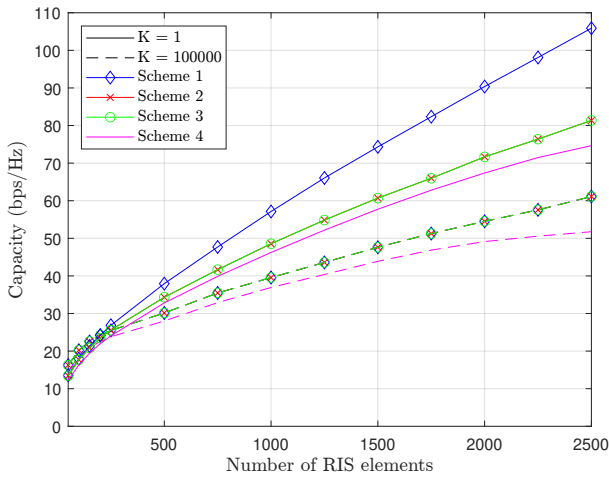


Fig. 2: Achievable rate as function of the number of RIS elements N .

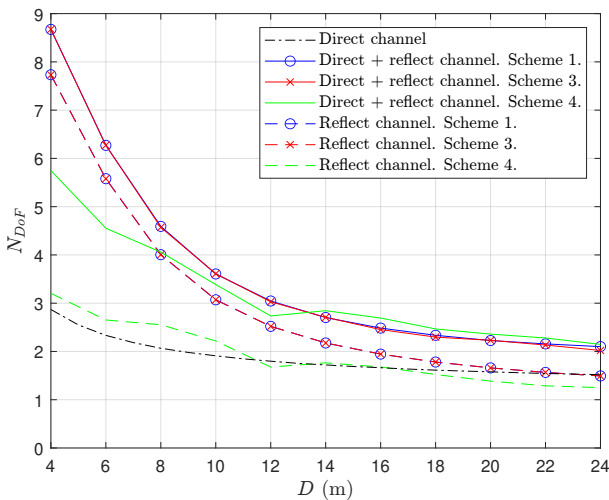


Fig. 3: DoF as a function of the transmission distance.

to note that a high rate is obtained even in LoS conditions ($K = 100,000$), thanks to the spherical wavefront under the considered setup. Specifically, we note that the rate obtained for low values of RIS elements is in agreement with the rate of a single-input single-output channel with a received signal-to-noise-ratio that corresponds to the considered setup when the transmission distances are those between the center-points of the transmitter and the RIS, and the center-points of the RIS and the receiver. Notably, in addition, we see that Scheme 3 and Scheme 1 offer almost the same performance for large values of K (LoS conditions).

In Fig. 3, we illustrate the number of DoF when the size of the RIS is 50×50 unit cells. To evaluate the number of strongly coupled transmission modes, we plot the effective rank [22]. Also, we assume LoS conditions ($K = 100,000$). The obtained results clearly show that the deployment of an RIS can extend the near-field region between the transmitting and receiving HoloS, to an extent that the end-to-end channel has a number of DoF that exceeds the number of DoF of

the direct link, especially if the distance D is small enough compared with the sizes of the transmitting and receiving HoloS and the RIS. Once again, Scheme 3 provides almost the same number of DoF as Scheme 1. As expected, the number of DoF tends to one when the transmission distance is large.

For illustrative purposes, it is interesting to visualize the shape of the optimal spatial functions (communication modes) at the transmitting HoloS when they are observed at the RIS. In mathematical terms, we plot the following:

$$\mathbf{w}_i = \mathbf{H}\mathbf{v}_i\sqrt{P_{T_i}} \quad (34)$$

where \mathbf{v}_i corresponds to the i -th column of the matrix \mathbf{V} .

In Fig. 4, we show \mathbf{w}_i for the six strongest communication modes when the direct channel is blocked and $D = 6$ m.

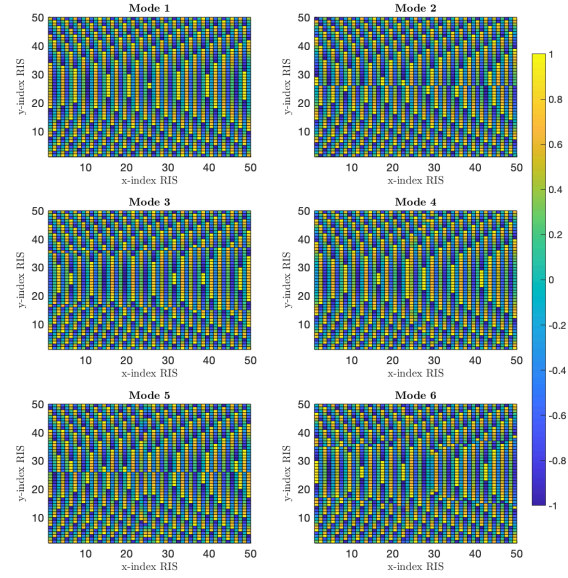
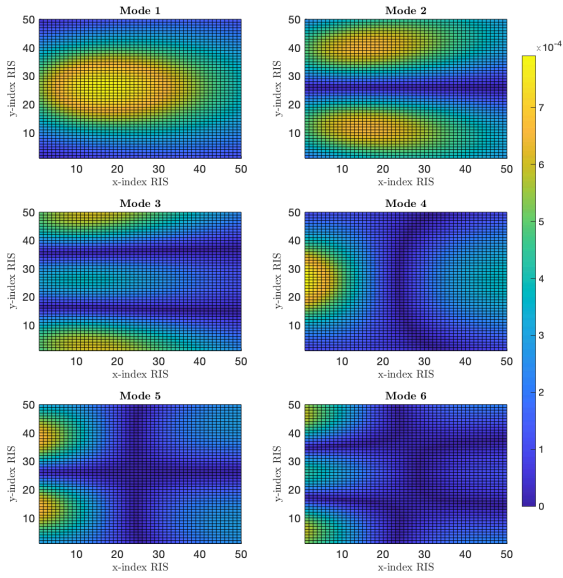
Finally, we analyze how the position of the RIS impacts the number of DoF. This is shown in Fig. 5 for $D = 10$ m. We note that the number of effective (strongly coupled) DoF fluctuates slowly with the position of the RIS.

V. CONCLUSIONS

In this paper, we have analyzed the performance of RIS-aided HoloS communications in terms of rate and DoF. We have compared different case studies as a function of the CSI prior knowledge for optimizing the phase shifts of the RIS. The main finding of this paper is that optimizing an RIS based only on location information offers good performance, provided that the channels are predominantly in LoS conditions. This is often the case in high frequency channels, e.g., sub-terahertz and terahertz channels, due to the lack of diffraction.

REFERENCES

- [1] E. C. Strinati, G. C. Alexandropoulos, V. Sciancalepore, M. Di Renzo, H. Wymeersch, D.-T. Phan-Huy, M. Crozzoli, R. D'Errico, E. De Carvalho, P. Popovski, P. Di Lorenzo, L. Bastianelli, M. Belouar, J. E. Mascolo, G. Gradoni, S. Phang, G. Lerosey, and B. Denis, "Wireless environment as a service enabled by reconfigurable intelligent surfaces: The rise-6g perspective," in *2021 Joint European Conference on Networks and Communications & 6G Summit (EuCNC/6G Summit)*, 2021, pp. 562–567.
- [2] D. Kitayama, D. Kurita, K. Miyachi, Y. Kishiyama, S. Itoh, and T. Tachizawa, "5G radio access experiments on coverage expansion using metasurface reflector at 28 GHz," in *2019 IEEE Asia-Pacific Microwave Conference (APMC)*, 2019, pp. 435–437.
- [3] R. Fara, P. Ratajczak, D.-T. Phan-Huy, A. Ourir, M. Di Renzo, and J. de Rosny, "A prototype of reconfigurable intelligent surface with continuous control of the reflection phase," *IEEE Wireless Communications*, vol. 29, no. 1, pp. 70–77, 2022.
- [4] B. Sihlbom, M. I. Poulakis, and M. Di Renzo, "Reconfigurable intelligent surfaces: Performance assessment through a system-level simulator," *IEEE Wireless Communications*, pp. 1–10, 2022.
- [5] H. Gacanin and M. Di Renzo, "Wireless 2.0: Toward an intelligent radio environment empowered by reconfigurable meta-surfaces and artificial intelligence," *IEEE Vehicular Technology Magazine*, vol. 15, no. 4, pp. 74–82, 2020.
- [6] M. Di Renzo, A. Zappone, M. Debbah, M.-S. Alouini, C. Yuen, J. de Rosny, and S. Tretyakov, "Smart radio environments empowered by reconfigurable intelligent surfaces: How it works, state of research, and the road ahead," *IEEE Journal on Selected Areas in Communications*, vol. 38, no. 11, pp. 2450–2525, 2020.
- [7] M. Di Renzo and J. Song, "Reflection probability in wireless networks with metasurface-coated environmental objects: an approach based on random spatial processes," *EURASIP J. Wirel. Commun. Netw.*, vol. 2019, p. 99, 2019.



(a) Absolute value of the communication modes.

(b) Phase (normalized by π) of the communication modes.

Fig. 4: Communication modes observed at the RIS.

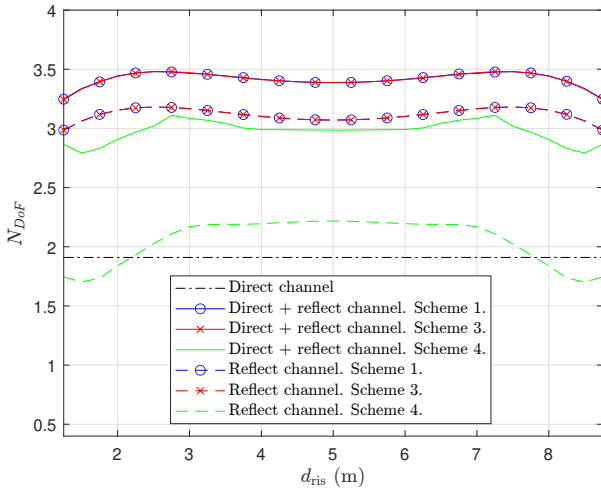


Fig. 5: Number of DoF as a function of the position of the RIS.

- [8] C. Huang, S. Hu, G. C. Alexandropoulos, A. Zappone, C. Yuen, R. Zhang, M. Di Renzo, and M. Debbah, "Holographic mimo surfaces for 6g wireless networks: Opportunities, challenges, and trends," *IEEE Wireless Communications*, vol. 27, no. 5, pp. 118–125, 2020.
- [9] M. Di Renzo, M. Debbah, D. T. P. Huy, A. Zappone, M. Alouini, C. Yuen, V. Sciancalepore, G. C. Alexandropoulos, J. Hoydis, H. Gacanin, J. de Rosny, A. Bounceur, G. Lerosey, and M. Fink, "Smart radio environments empowered by reconfigurable AI meta-surfaces: an idea whose time has come," *EURASIP J. Wirel. Commun. Netw.*, vol. 2019, p. 129, 2019.
- [10] Q. Wu, S. Zhang, B. Zheng, C. You, and R. Zhang, "Intelligent reflecting surface-aided wireless communications: A tutorial," *IEEE Transactions on Communications*, vol. 69, no. 5, pp. 3313–3351, 2021.
- [11] M. Di Renzo, D. Dardari, and N. Decarli, "LoS MIMO-Arrays vs. LoS MIMO-Surfaces," *IEEE European Conference on Antennas and Propagation*, 2023. [Online]. Available: <https://doi.org/10.48550/arXiv.2210.08616>

- [12] D. Tse and P. Viswanath, *Fundamentals of Wireless Communication*. USA: Cambridge University Press, 2005.
- [13] D. Dardari, "Communicating with large intelligent surfaces: Fundamental limits and models," *IEEE Journal on Selected Areas in Communications*, vol. 38, no. 11, pp. 2526–2537, nov 2020.
- [14] M. Di Renzo, F. H. Danufane, and S. Tretyakov, "Communication models for reconfigurable intelligent surfaces: From surface electromagnetics to wireless networks optimization," *Proceedings of the IEEE*, vol. 110, no. 9, pp. 1164–1209, 2022.
- [15] N. S. Perović, L.-N. Tran, M. Di Renzo, and M. F. Flanagan, "Achievable rate optimization for MIMO systems with reconfigurable intelligent surfaces," *IEEE Transactions on Wireless Communications*, vol. 20, no. 6, pp. 3865–3882, 2021.
- [16] A. Abrardo, D. Dardari, and M. Di Renzo, "Intelligent reflecting surfaces: Sum-rate optimization based on statistical position information," *IEEE Transactions on Communications*, vol. 69, no. 10, pp. 7121–7136, 2021.
- [17] C. Pan, G. Zhou, K. Zhi, S. Hong, T. Wu, Y. Pan, H. Ren, M. Di Renzo, A. Lee Swindlehurst, R. Zhang, and A. Y. Zhang, "An overview of signal processing techniques for ris/rirs-aided wireless systems," *IEEE Journal of Selected Topics in Signal Processing*, vol. 16, no. 5, pp. 883–917, 2022.
- [18] N. S. Perović, L.-N. Tran, M. Di Renzo, and M. F. Flanagan, "Optimization of RIS-aided MIMO systems via the cutoff rate," *IEEE Wireless Communications Letters*, vol. 10, no. 8, pp. 1692–1696, 2021.
- [19] D. A. B. Miller, "Communicating with waves between volumes: evaluating orthogonal spatial channels and limits on coupling strengths," *Appl. Opt.*, vol. 39, no. 11, pp. 1681–1699, Apr. 2000. [Online]. Available: <https://opg.optica.org/ao/abstract.cfm?URI=ao-39-11-1681>
- [20] G. Bartoli, A. Abrardo, N. Decarli, D. Dardari, and M. Di Renzo, "Spatial multiplexing in near field MIMO channels with reconfigurable intelligent surfaces," 2022. [Online]. Available: <https://arxiv.org/abs/2212.11057>
- [21] H. Do, N. Lee, and A. Lozano, "Line-of-sight MIMO via intelligent reflecting surface," *IEEE Transactions on Wireless Communications*, pp. 1–1, 2022.
- [22] O. Roy and M. Vetterli, "The effective rank: A measure of effective dimensionality," in *2007 15th European Signal Processing Conference*, 2007, pp. 606–610.